

Article

# Finite Element Analysis of Laser Peening of Thin Aluminum Structures

Kristina Langer <sup>1</sup>, Thomas J. Spradlin <sup>1</sup> and Michael E. Fitzpatrick <sup>2,\*</sup> 

<sup>1</sup> Air Force Research Laboratory, Wright-Patterson Air Force Base, OH 45433, USA; kristina.langer@us.af.mil (K.L.); thomas.spradlin.1@us.af.mil (T.J.S.)

<sup>2</sup> Faculty of Engineering, Environment, and Computing, Coventry University, Coventry CV1 5FB, UK

\* Correspondence: Michael.Fitzpatrick@coventry.ac.uk or ab6856@coventry.ac.uk

Received: 20 September 2019; Accepted: 2 December 2019; Published: 6 January 2020



**Abstract:** Laser shock peening has become a commonly applied industrial surface treatment, particularly for high-strength steel and titanium components. Effective application to aluminum alloys, especially in the thin sections common in aerospace structures, has proved more challenging. Previous work has shown that some peening conditions can introduce at-surface tensile residual stress in thin Al sections. In this study, we employ finite element modeling to identify the conditions that cause this to occur, and show how these adverse effects can be mitigated through selection of peen parameters and patterning.

**Keywords:** laser peening; residual stress; aluminum alloys

## 1. Introduction

Over the past three decades, laser peening (LP) has emerged as a viable commercial technology for introducing beneficial residual compression into the near-surface regions of metallic components [1,2]. First introduced by Battelle Laboratories, Columbus, Ohio, in the 1970s [3,4], LP uses a high-power-density, short-duration pulsed laser to create a mechanical impact on the surface of a component. The amplitude of the impact, typically at least double the Hugoniot elastic limit (HEL) of the target material, is great enough that the resultant shock wave creates a region of localized plastic deformation in the target material. The elastic springback of the surrounding material around this plastic core creates a state of self-equilibrating residual stress in the component. Good reviews of the LP process can be found in [5–7].

Because the depth of compression resulting from an LP treatment is typically on the order of 1 mm or greater, depending on the component material, geometry, and selected peening parameters, LP has the potential to significantly mitigate fatigue-inducing tensile stresses that can result from applied cyclic loading. This is of particular interest as a potential means for enhancing the fatigue response of military aircraft in which mission changes and extended lifing requirements often tax the fatigue resistance of the airframes beyond their original design specifications [8].

One application of recent interest is LP of thin aluminum components, on the order of 2–3 mm or less such as aircraft skin or web structure, to mitigate surface damage or enhance fatigue response. If LP parameters and process variables are designed appropriately, a favorable compressive state throughout much of the component depth can be induced [9]; however, as is discussed in more detail below, under certain circumstances LP can also induce detrimental tensile stresses into the near-surface regions of thin sections, extending into the component to depths as great as 0.5 mm [10–12].

A number of factors can contribute to the challenge of developing favorable residual stress states in thin structures: First, if the laser power density and subsequent plasma pressure are too high, the resulting distortion in the thin section can reduce the magnitude of the compressive stresses [9,13].

Second, even in the absence of significant distortion, the limited depth of material along the propagation direction of the shock wave constrains the induced plastic field, which in turn can limit the magnitude of the residual stresses. Third, because the plastic wave will typically not completely attenuate through the material depth, reflected waves from the opposite free surface can form, with the effect of altering the residual stresses from compressive to tensile [14]. Fourth, the work hardening resulting from LP affects a greater percentage of the depth of a thin component than a thicker one, and can therefore impact the development of the residual stress fields and also the fatigue response [15]. Finally, the rolling process typically used to produce thin plates induces a crystallographic texture that can influence the development of residual stresses [16].

In early studies, some of these thin section challenges were addressed by splitting the laser beam to peen both sides of the plate simultaneously [9]. While this technique was designed to help minimize overall distortion, the mid-plane collision of the two compressive shock fronts resulted in detrimental, high-magnitude internal tensile stresses [17]. In addition, for many in situ components, such as an aircraft skin, implementation of two-sided peening is not feasible.

More recently, Dorman et al. [10] investigated the use of LP to treat surface scribe marks on thin Al 2024-T351 sheets. Specimens were peened from one side only, with a single layer of square spots patterned in either a line overlaying the scribe mark or a patch covering it, and using an ablative coating on the peen surface and an acoustic damping material on the back surface. The resulting residual stresses were then measured using incremental hole drilling and synchrotron X-ray diffraction. In all cases—regardless of the depth of the scribe mark, the use of an ablative layer, or the intensity of the peening—the near-surface residual stress, measured in the center of the peen spots normal to the peen line, was either tensile or only slightly compressive. The tensile stresses persisted to subsurface depths ranging from 80  $\mu\text{m}$  at the lowest laser power density to 320  $\mu\text{m}$  at the highest, with magnitudes reaching as high as 100 MPa. In addition, in all cases in which the peening pattern was a single line, the resultant residual stress fields were strongly non-biaxial, with higher compression parallel to the peen line axis than in the transverse direction.

Cellard et al. [15] noted similar results in their measurements of LP-induced residual stresses in very thin (1 mm) Ti-17 plates. The specimens were peened from one side only using square laser spots of varying size, intensity, duration, and coverage. Using X-ray diffraction to measure the surface residual stresses, they found that nearly all of the thin specimens had some level of tension at the surface, ranging from 13 to 150 MPa. When the same peening parameters were applied to thick specimens (9 mm), however, nearly all demonstrated compressive residual stress on the surface. They attribute this “thickness effect” to the redistribution of stresses required to maintain equilibrium over a cross-section of the specimen, and suggested that two-sided peening could yield more favorable stress fields in thin specimens.

In contrast, several researchers studying the effects of LP in aluminum sheet have not observed tensile stresses at the surface. Hong and Chengye [18] and Yang et al. [19] peened 2.5-mm-thick Al2024 and observed compressive surface stresses at the centers of round LP spots using conventional XRD. However, as noted in [16], surface XRD measurements can be distorted by rolling-induced texture and thus a secondary stress measurement technique is recommended to reduce uncertainties. Ivetic et al. [20] studied the effects of LP on slightly thicker Al 6082-T6 plates, 3 mm in thickness, and measured near-surface compression using synchrotron X-ray diffraction. However, the depth at which the measurements were recorded was slightly subsurface, 50–250  $\mu\text{m}$ , so that any tensile stresses that might have formed in shallower regions might not have been detected.

In the present work, three-dimensional non-linear finite element modeling is used to investigate the effects of laser peening on residual stresses in thin aluminum plates. We explore the relationship between spot layering and peen patterning, with the objective being to better understand the effects of processing technique on the resulting residual stress fields.

## 2. LP Process Modeling

Owing to its flexibility and relative ease of use, finite element analysis (FEA) has emerged as a powerful tool for predicting the full residual stress state that results from the laser peening of an arbitrary three-dimensional metallic body. First used by Braisted and Brockman [21] to simulate single LP shots on semi-infinite bodies, FEA techniques have evolved significantly over the past decade as computer processing has become faster and multiprocessing environments have become mainstream. Recent FEA studies of note include the work of Ding and Ye [22], who used three-dimensional FEA to create detailed stress maps for LP steel; Ocaña et al. [23], who developed a multi-shot FEA model capable of realistic LP simulation; Singh et al. [24], who coupled FEA with numerical optimization; Brockman et al. [25], who used a highly refined, fully three-dimensional model to study local variations in surface residual stresses arising from shot patterning; and Hasser et al. [26], who developed a first-ever FEA capability for studying LP-induced surface roughness.

In the present work, a series of finite element analyses were performed using the commercial FEA package Abaqus [27]. The objective of the analyses was to explore computationally the effects of various peening parameters and processing variables on the resulting residual stress fields in thin structures in order to better understand the experimental findings discussed in the previous section: (1) the formation of surface tensile stresses in spot centers that tend to occur in thin plates but not thicker sections, (2) the observed inequality of the residual stresses that occur parallel to and perpendicular to a peen line, and (3) the effects of peen patterning on the resulting stress fields.

The key aspects in using FEA to model an LP shock event are the selection of appropriate input models, namely the material model and the pressure model, and selection of a computational strategy and associated computational parameters that provide for an accurate and efficient solution. In this section, we discuss the material model used to capture high-strain-rate effects, the pressure model used to approximate the laser-induced plasma impact, and the computational model used to develop the stress predictions.

### 2.1. LP Process

The basic LP process is illustrated in Figure 1. In typical applications, an ablative coating, such as aluminum tape or black paint, along with a transparent overlay, usually water, are applied to the surface of the target material prior to peening. When used together, the confined ablation increases the intensity of the plasma pressure, which results in a higher intensity shock wave in the target material. During the peening process, the component is exposed to a very high intensity (1–9 GW/cm<sup>2</sup>) laser pulse, typically from an Nd:YAG or Nd:glass laser system operating at a FWHM of about 6–30 ns per pulse with a beam dimension of less than 10 mm [6,28].

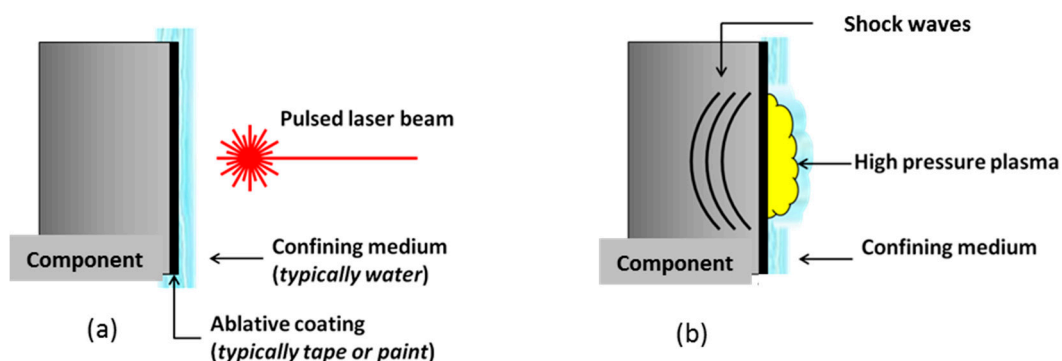


**Figure 1.** (a) A high-intensity, pulsed laser vaporizes an ablative layer on the surface of the component, producing a rapidly expanding plasma. (b) The plasma is constrained by a confining medium, which creates a high-amplitude pressure pulse and induces a shock wave in the component.

The resulting pressure pulse generally lasts about 2–3 times the duration of the laser pulse and has a peak magnitude of about 1–10 GPa [28]. The spatial distribution of the plasma pressure can either be uniform or variable, depending upon the laser system employed. In order to generate the near-surface plasticity required to induce a residual stress, the plasma pressure needs to exceed the HEL of the target material for a sufficient amount of time, with an optimal value typically about 2–2.5 times the HEL [29].

## 2.2. Computational Model

The commercial finite element package ABAQUS [27] was used to solve for the stresses, strains, and displacements that result from the application of laser peening on thin sheets of Al2024-T351. Based on previous work [11,25,30–33], all simulations were run using explicit time integration (ABAQUS/Explicit) to solve the dynamic system. As discussed in [25], using an explicit solver to model both the impact event and the subsequent return to equilibrium is quicker, more scalable, and uses less memory than performing the equilibrium analysis with an implicit solver. Each impact pulse was modeled using two distinct solution steps so that the computational parameters could be adjusted for improved efficiency and convergence. The first solution step, designated as the pulse phase, starts with the initial application of the pressure pulse and ends when no further plastic deformation occurs (2.5  $\mu\text{s}$  was used). The second solution step, termed the equilibrium phase, introduces Rayleigh damping [34] into the model to return the system to a state of near-zero kinetic energy (approximately  $10^{-6}$  to approximate equilibrium: 100  $\mu\text{s}$  was used). One pair of analyses is performed for each laser pulse.

Three-dimensional linear eight-node brick elements with reduced integration (C3D8R in Abaqus terminology) were used throughout, with a mesh size of 50  $\mu\text{m}$  in the laser peened region. This mesh size was selected using the results of convergence studies that showed less than 2% difference in predicted residual stresses with further refinement. External to the peened region the element size was increased gradually from 50  $\mu\text{m}$  to 250  $\mu\text{m}$  using mesh biasing to curtail computational costs.

## 2.3. Material Model

During the laser peening process, the induced shock waves can produce very high strain rates, on the order of  $10^6 \text{ s}^{-1}$ , resulting in a material response that is significantly different from that under static or quasi-static loading conditions [35]. To capture these strain rate effects, a Johnson–Cook [36] material model was used. Following earlier work [11], thermal effects resulting from the LP process are considered to be negligible and thus temperature dependence is eliminated from the material model:

$$\bar{\sigma} = \left[ A + B(\bar{\epsilon}^p)^n \right] \left[ 1 + C \ln\left(\frac{\dot{\epsilon}^p}{\dot{\epsilon}_0}\right) \right] \quad (1)$$

Here,  $\bar{\sigma}$  is the flow stress;  $\bar{\epsilon}^p$  is the effective plastic strain;  $\dot{\epsilon}^p$  is the effective plastic strain rate;  $\dot{\epsilon}_0$  is a reference plastic strain rate (typically taken to be  $1.0 \text{ s}^{-1}$ );  $n$  is the work hardening exponent; and  $A$ ,  $B$ , and  $C$  are empirically-derived constants.

Lesuer [37] used split-Hopkinson-bar testing to measure the deformation response of Al 2024-T3 at moderately high strain rates ( $10^3$ – $10^4 \text{ s}^{-1}$ ), and used the data to define the material constants in Equation (1) (Table 1). Although the strain rates typically experienced during LP are an order of magnitude higher, recent flyer-plate testing has confirmed that Lesuer’s constants reasonably model the LP material response, with a maximum deviation of less than 10% as compared to the measured values [38]. Comparisons between predicted residual stresses based on a Johnson–Cook material model and measured values have also validated the use this mode for LP simulations [39,40]. Thus, the Johnson–Cook material constants for Al 2024-T3 as shown in Table 1 were used for all simulations in the current work.

**Table 1.** Johnson–Cook material constants [37].

Material	A/MPa	B/MPa	C	n
Al 2024-T3	369	684	0.014	0.93

It should be noted that the constitutive model was not updated in the multi-shot simulations to account for LP-induced cyclic deformation effects [41].

#### 2.4. Pressure Model

In this work, the laser-matter interaction and subsequent plasma formation were not modeled directly; rather, the resulting pressure pulse was applied to the FE model over the area corresponding to the laser pulse as a spatially-uniform, time-varying surface traction. While small transition regions likely exist along the spot perimeters, measurements by the LP vendor indicate the generated pressures are essentially uniform across the spot area.

The confined ablation model developed by Fabbro et al. [42], modified to account for the absorption fraction of the laser energy in the treated plasma, was used to determine the applied pressure  $P(x,t) = P(t)$ . We can express the energy density at the plasma,  $E(t)$ , to the nominal energy density of the laser,  $I(t)$ , using the expression  $E(t) = A(t)I(t)$ , where  $A(t) = 1 - R(t)$  is the absorbed energy and  $R(t)$  represents the change in energy density. However, owing to the very short time between the laser pulse and the plasma formation, it is generally assumed that the loss  $R(t)$  is negligible and hence  $A(t)$  is approximately 1.0 [43–46].

During the heating phase (while the laser is on), this relationship is then described by:

$$E(t) = P(t) \frac{dL}{dt} + \frac{3}{2\alpha} \frac{d}{dt} [P(t)L(t)] \quad (2)$$

while during the cooling phase (after the laser is switched off):

$$P(t) = P(\tau) \left( \frac{L(\tau)}{L(t)} \right)^\gamma \quad (3)$$

Here,  $L(t)$  is the thickness at time  $t$  of the interface between the ablative coating and the transparent overlay, given by:

$$\frac{dL(t)}{dt} = \frac{2}{Z} P(t) \quad (4)$$

and  $\alpha$  is the fraction of the internal energy transferred to the workpiece,  $\gamma$  is the adiabatic cooling rate, and  $Z$  is the effective acoustic impedance of the interface, defined by:

$$\frac{2}{Z} = \frac{1}{Z_{\text{coating}}} + \frac{1}{Z_{\text{overlay}}} \quad (5)$$

$Z_{\text{coating}}$  and  $Z_{\text{overlay}}$  are the acoustic impedances of the ablative coating and the transparent overlay, respectively. With water as the overlay ( $Z_{\text{overlay}} \approx 0.15 \times 10^6 \text{ g cm}^{-2} \text{ s}^{-1}$ ) and aluminum tape as the coating ( $Z_{\text{coating}} \approx 1.7 \times 10^6 \text{ g cm}^{-2} \text{ s}^{-1}$ ),  $Z$  has a value of about  $0.3 \times 10^6 \text{ g cm}^{-2} \text{ s}^{-1}$ .

Assuming a Gaussian laser energy density  $E(t)$ , a typical pressure profile resulting from these equations is shown in Figure 2 for a maximum energy density of  $3 \text{ GW/cm}^2$ , laser pulse width of 18 ns,  $\alpha = 0.09$ , and  $\gamma = 1.3$ . For these parameters, the maximum applied pressure,  $P_{\text{max}}$  is about 1.95 GPa and the width (FWHM) of the pressure pulse is about 47 ns.

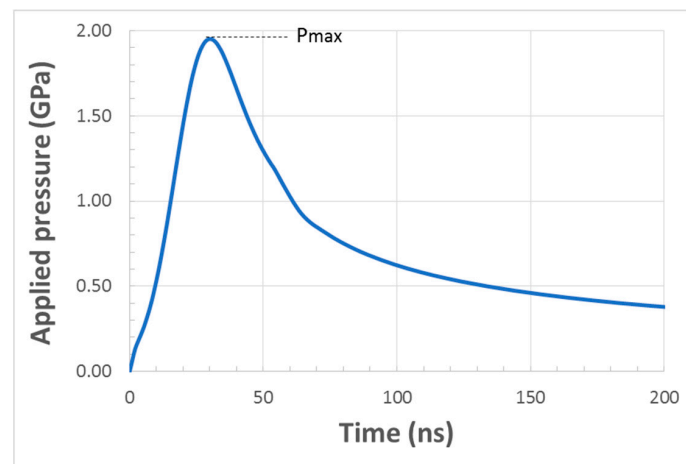


**Figure 2.** Typical temporal profile of the applied peening pressure.

### 2.5. Model Confirmation

Residual stress predictions using the model discussed in the previous sections were compared against experimental stress measurements. From previous studies, the value of  $\alpha$  was set to 0.09 and  $\gamma$  was 1.3. The measured residual stress profiles were extracted from two laser-peened test samples of 12.7-mm-thick Al2024-T351 aluminum (unclad) using incremental hole drilling (IHD). The IHD diameter was 2 mm and the depth increments ranged from 32 to 128  $\mu\text{m}$  to a total hole depth of 1408  $\mu\text{m}$ . Each sample (IHD-1 and IHD-2) was peened with a single 5 mm  $\times$  5 mm square spot located sufficiently far from the boundaries to avoid edge effects and using a power density of 3 GW/cm<sup>2</sup> and a pulse width of 18 ns. The residual stresses were measured at the spot center.

Results from the comparison are shown in Figure 3. The FE results represent the average principal stresses over the equivalent volume of material removed at each IHD step and are reported depthwise at the center of the IHD increment. Numerical integration over the disk-shaped IHD region was used to compute the averages. As is shown, the predicted stresses agree well with the stress measurements, confirming the performance of the model for LP applications.

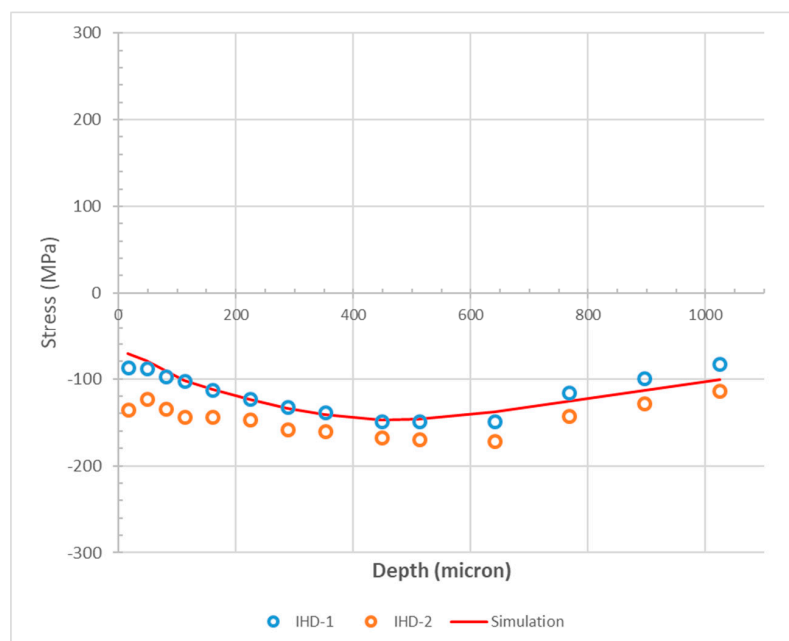


**Figure 3.** Comparison of predicted residual stresses against measured values.

### 3. Results and Discussion

The FEA model developed in the previous section was used to investigate the stress distributions resulting from different peening schemes in order to better understand how combinations of peening parameters influence residual stress distributions in thin sections. Only one-sided peening without a backing material was considered, reflecting the potential future application of in situ treatment of thin aircraft components. All simulations used a 5 mm × 5 mm square laser spot.

In general, a favorable state of residual stress for mitigating fatigue has several key characteristics. First, sufficient compression should exist at the surface and in the near-surface regions of critical areas of the component to offset fatigue-inducing tensile stresses. Second, the distribution and magnitude of the compensatory tension that arises from the LP process should not initiate a failure event when fatigue loads are applied. Third, for a line of peen spots that align with and overlay a surface scratch, such as the geometry considered in [10,12], near-surface tensile stresses transverse to the peen line should be absent to prevent premature initiation of a crack from the scratch.

#### 3.1. Single Shot Simulations

Simulations of a single LP shot were used to develop a better understanding of the shock response of laser-peened thin plates under different peening conditions. All thin-section simulations were run on a 2-mm-thick plate of Al2024-T351 (unclad), with the peened area located sufficiently far from the plate boundaries to avoid the effects of reflected waves. Note that due to symmetry, only one half of the plate was modeled.

##### 3.1.1. Effects of Peening Pressure

Figure 4 shows the effects of varying the applied pressure for a single layer of peening with a fairly large (5 × 5 mm<sup>2</sup>) square spot. The contour plots represent a cross-section of the plate taken through the spot center, with the colors representing the range of the in-plane stress component  $S_{22}$  normal to the cross-sectional surface. Line plots of stress as a function of depth through the spot center are also shown. Note that in these plots, in contrast to the plots in Figure 3, the stresses are not averaged over a volume; rather, they are extracted directly from the element integration points.

At low pressures (Figure 4a), less than about twice the HEL, surface tensile stresses are absent in the spot center. However, the magnitude of the maximum compressive stress is fairly low and fairly shallow—only about 80 MPa that tapers out after about 0.5 mm depth—and tensile stress persists through the thickness reaching about 60 MPa at a depth just over three-quarters of the way through the thickness.

At pressures about twice the HEL (Figure 4b), small tensile zones appear in the spot centers similar to the experimental findings in [10]. The magnitude of the stress at the surface is about 100 MPa, and the tension persists in a region around the spot center that measures about 250 μm at the surface and extends about 35 μm subsurface. The maximum compressive stresses in this pressure regime are greater than those realized at lower pressures, reaching about −130 MPa, but are not significantly deeper (about 100 μm). It should be noted that the size of the tensile zones predicted by these simulations are generally smaller than what was reported in [10]. This likely results from the pressure pulse approximation assumption of a spatially uniform distribution along with averaging effects in the experimental values.

Increasing the applied pressure to three times the HEL (Figure 4c) increases the size of the surface tensile zone slightly but also drives the compressive stresses deeper into the component thickness. Near to the spot centerline the compression persists throughout the plate thickness; however, the stress state is not uniform across the spot width, with tensile pockets forming subsurface around the compressed region. At very high applied pressures, about four times the HEL (Figure 4d), through-thickness compression is no longer achievable, with tensile stresses forming at the back surface.

It should be noted that the specific results for this series of single-shot simulations depend on not only the maximum applied pressure, but also on the shape and length of the pressure pulse and the thickness of the plate. For thicker or thinner sheets, and for different pulse shapes, the precise points at which the nature of the residual stresses change will vary; however, the basic trends are similar.

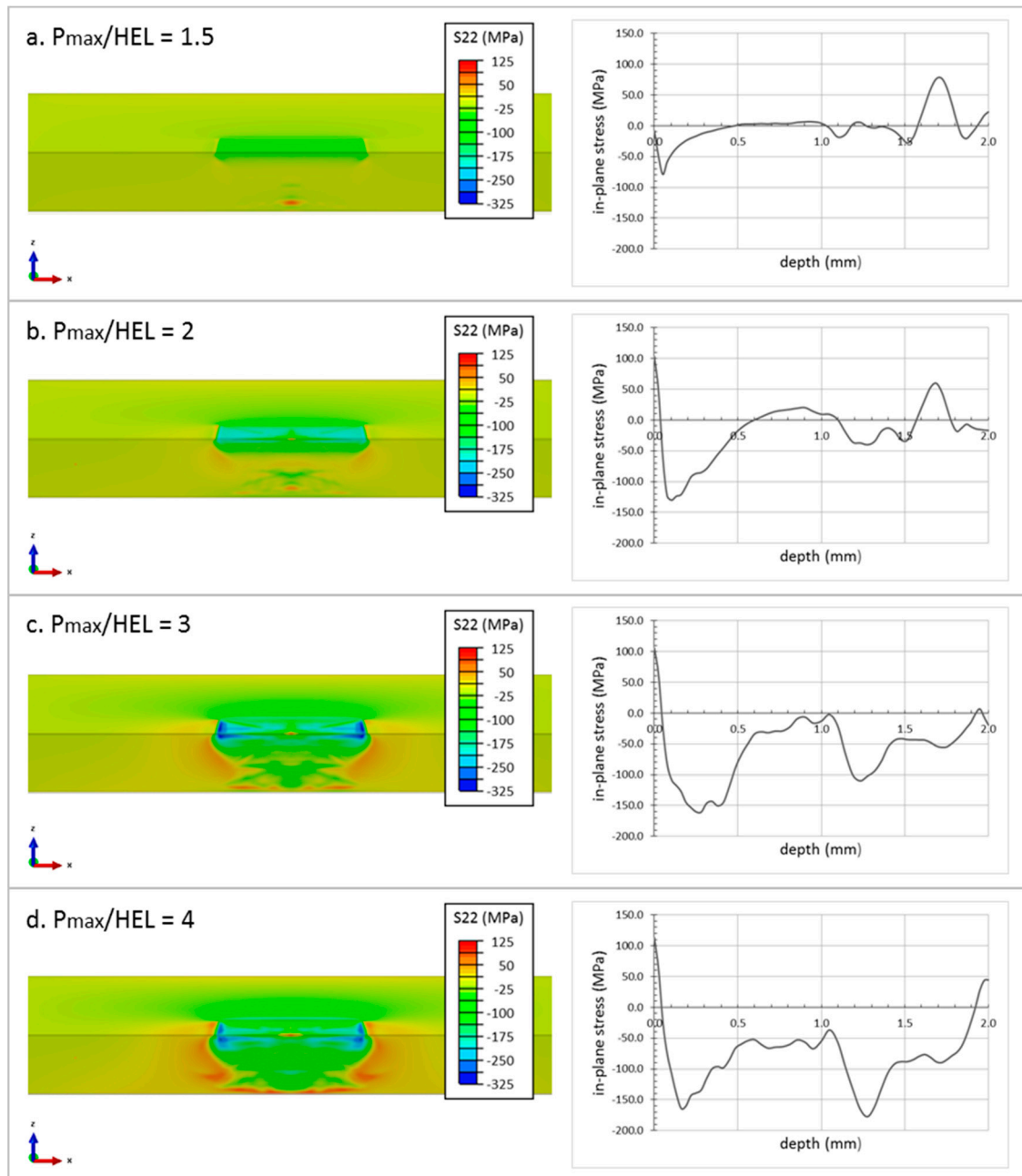


**Figure 4.** Finite element analysis (FEA)-computed in-plane residual stress from a single square laser peening (LP) shot ( $5 \times 5 \text{ mm}^2$ ) on a 2-mm-thick Al2024-T351 plate at various pressure levels.

A comparison between the LP response of a thicker plate (10 mm) and the response of a thin section (2 mm) is shown in Figure 5. Both simulations used a maximum applied pressure of 2.5 times the HEL, with the plate thickness as the only difference. As can be seen from the line plot in Figure 5, the near-surface tensile stresses around the spot center in the thin section are completely absent from the thick section. In addition, because the thick section does not experience stress reversals resulting

from wave reflections off the back surface, the maximum residual compressive stresses are significantly greater in magnitude than that of a thin section, by a factor of about two.

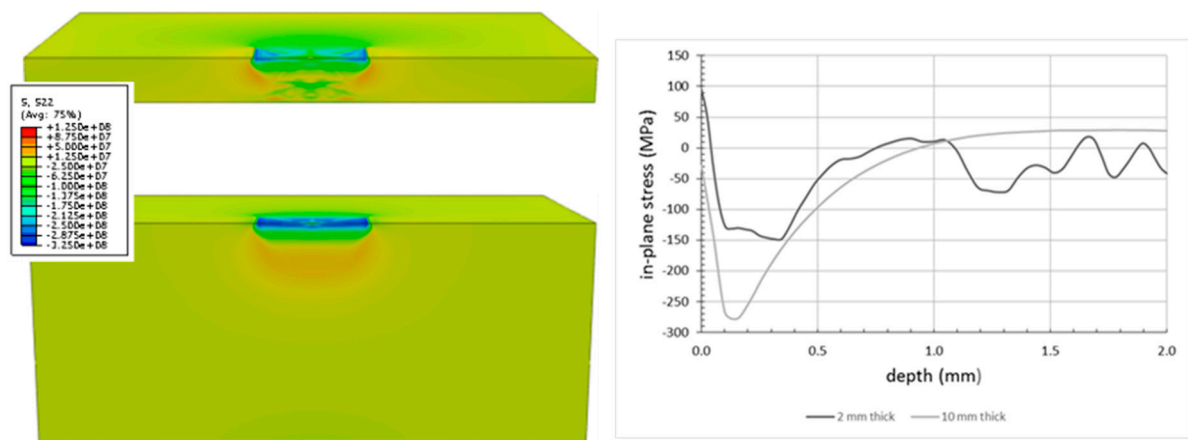


**Figure 5.** Effect of plate thickness on predicted in-plane residual stress (single square LP shot,  $5 \times 5$  mm<sup>2</sup>, on a 2-mm-thick Al2024-T351 plate).

### 3.1.2. Effects of Peen Layers

When additional layers of peening are considered on a thin section, as shown in Figure 6, the near-surface tensile stresses are mitigated. For the case shown, with an applied pressure of 2.5 times the HEL, a second layer of peening reduces the size and magnitude of the surface tensile field by more than 50%. Adding a third layer of peening completely suppresses the near-surface tension and a fourth layer drives the surface into compression. The maximum subsurface compressive stress is only minimally affected by additional layers, increasing by less than 50 MPa from one layer to four, but the depth of compression more than doubles. At the same time, however, the additional peen layers result in larger tensile stresses on the back surface.

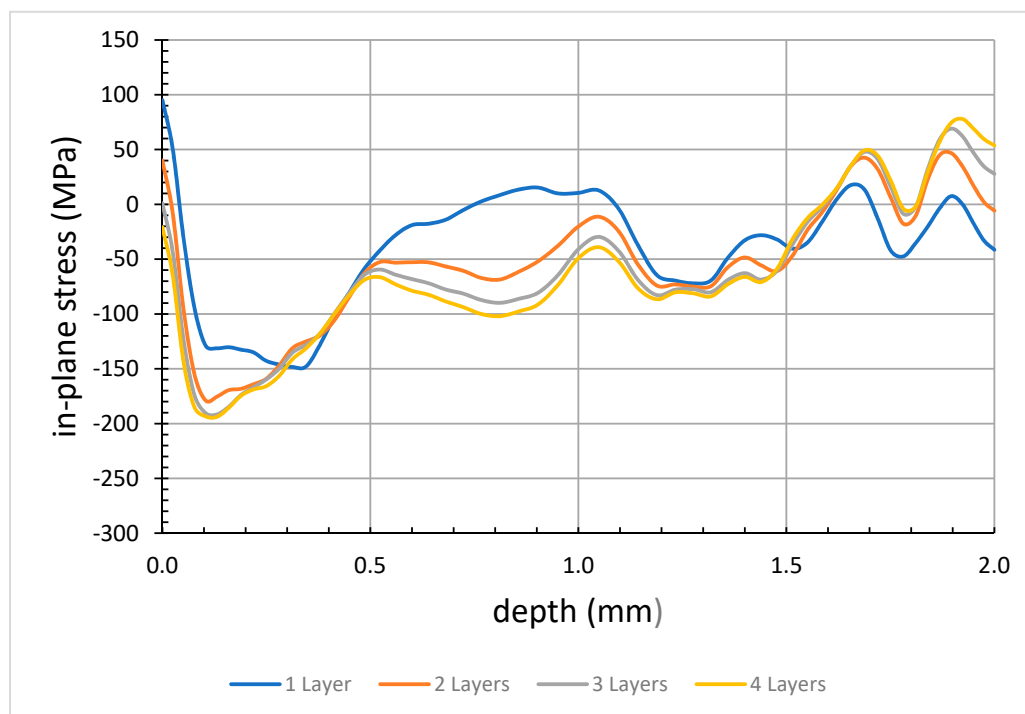


**Figure 6.** Effect of peen layering on predicted in-plane residual stress in thin sections (single square LP shot,  $5 \times 5$  mm<sup>2</sup>, on a 2-mm-thick Al2024-T351 plate).

### 3.1.3. Observations

It should be noted that in all single-shot simulations, the predicted in-plane residual stresses are equi-biaxial, as would be expected due to symmetry. The  $S_{22}$  stresses in the plane normal to the  $y$ -axis are equivalent to the  $S_{11}$  stresses in the plane normal to the  $x$ -axis.

The results of these single-shot simulations suggest that a favorable state of residual stress in thin sections can be realized by selecting a peening pressure high enough to achieve the desired compression without the detrimental subsurface tensile stresses, along with sufficient peen layers to suppress the near-surface tension. As discussed in the following sections, however, a third parameter, namely, the peen patterning, can also strongly influence the resulting stresses in thin sections, and, as will be discussed, observations for single shots do not necessarily hold in multi-shot scenarios.

## 3.2. Simulation of a Peened Line

Although the single shot simulations provide insight into the effects of applied pressure and layering, they cannot capture the interactions between adjacent and overlapping spots, or the effects of shot order and patterning. To investigate these effects, the FEA model used for the single shot simulations—a 2 mm thick plate of Al2024-T351—was extended lengthwise to accommodate the simulation of peened line under various peening conditions.

### 3.2.1. Effects of Adjacent Spots

Figure 7 shows the simulation results for a scenario similar to that considered in [10], namely, a single layer of peen spots applied edge-to-edge along a line with minimal overlap. The applied pressure used in the simulations was 2.5 times the HEL. As is shown, the center of each peen spot in the line exhibits a surface tensile stress normal to the peen line with a magnitude of about 110 MPa and extending about 50  $\mu\text{m}$  subsurface. The corresponding stress for a single peen spot is shown for comparison. Although the magnitude of the surface tensile stress is similar for the single spot and the peen line, the magnitude of the maximum compression resulting from the line configuration is about 20% lower than that of a single spot. The overall depth of compression is smaller in the line configuration as well, by about 0.25 mm.

Although the near-surface tensile stresses are contained only in the central regions near the spot center, significant tension (with a peak value of about 100 MPa) builds up subsurface in the regions between adjacent spots. For many fatigue applications these large subsurface tensile stresses can be undesirable, as they can lead to subsurface crack initiation that is undetectable by visual inspection of the component surface.

Figure 7 also compares the through-thickness profiles for the in-plane stresses taken parallel to ( $S_{11}$ ) and transverse to ( $S_{22}$ ) the peen line; as is shown, the stress states in the two directions are noticeably different, with as much as a 50 MPa variation in some locations. In general, the stresses transverse to the peened line are less compressive (or more tensile) than those in the longitudinal direction. This could pose a concern for certain applications in which the peen line was designed to overlay a surface scratch. Because the stresses are of lower magnitude (or even more tensile) in the critical direction (i.e., the direction that would tend to encourage crack formation and opening), the true potential of the LP treatment would not be realized, and could even exacerbate the situation. It should also be noted that through the spot centers, the stresses transverse to the peen line are generally more tensile than those predicted by single shot simulations.

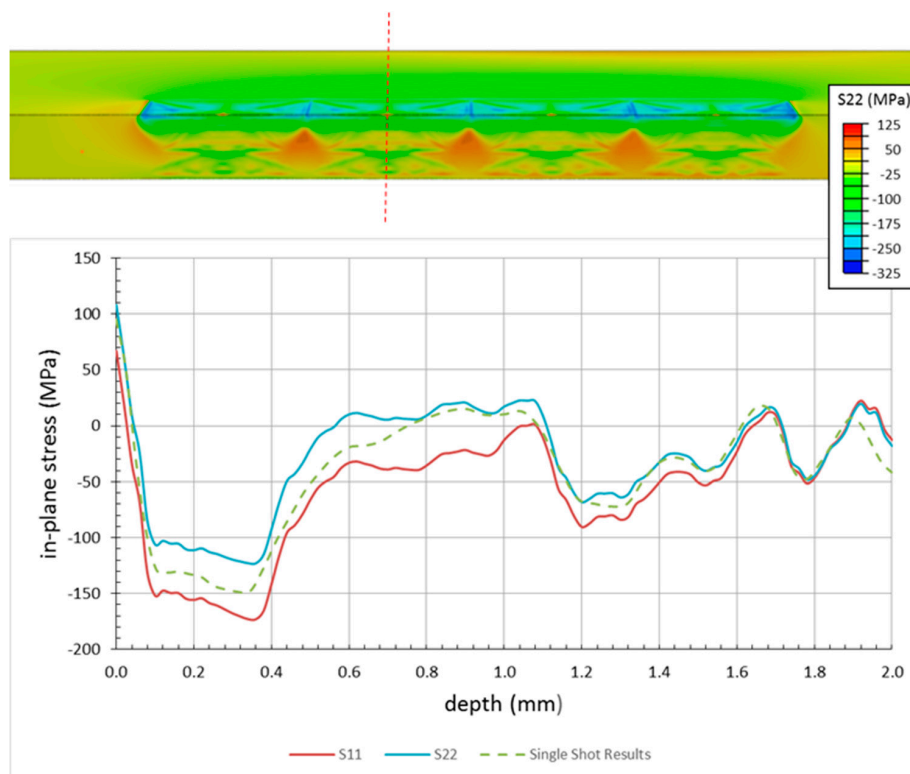


**Figure 7.** Comparison of stress profiles between a single peen spot and a peen line.

### 3.2.2. Effects of Peen Layers

As was the case for single shots, augmenting the peen line with additional layers can help alleviate the surface tensile stresses at the spot centers. In Figure 8, second and third layers of peen spots are applied along the peen line at a 50% offset between one layer and the next, as shown in the schematic. The line plots illustrate the in-plane stress through the center of a spot on the topmost layer (denoted Location L1). Similar to the case of a single peen spot, the surface tensile zones in the spot centers are reduced as additional layers are applied; however, the effects of adjacent spots are very apparent. A second layer flips the surface stress to compression (from 108 MPa to  $-243$  MPa) while a third layer flips it again (from  $-243$  MPa to 46 MPa). The end result is that although the stress at this location is reduced with additional peen layers, shallow tensile regions—about  $20\ \mu\text{m}$  deep and  $20\ \mu\text{m}$  in width—persist in the center of each spot that comprises the topmost layer of the plate.

It should be noted that while Figure 8 suggests that limiting the peening to two layers would alleviate the surface tensile stress at Location L1, detrimental stresses form elsewhere. Figure 9 illustrates this by extracting stress plots at location L2 after one and two layers of peening. As is shown, the surface stress at this location decreases more than 50% with the addition of the second layer (from 108 MPa to 48 MPa), but the tension persists.

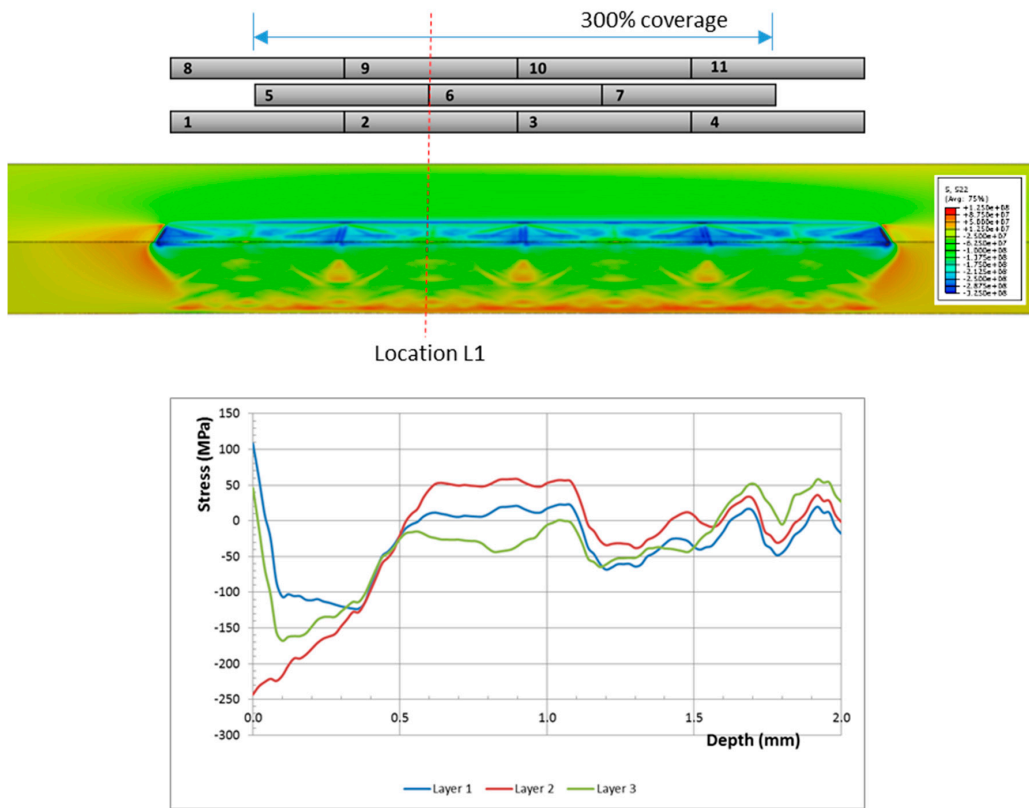


**Figure 8.** Effect of peen layering on predicted in-plane residual stress in thin sections. Stresses were extracted from the FEA model at Location L1 after one, two, and three layers of peening.

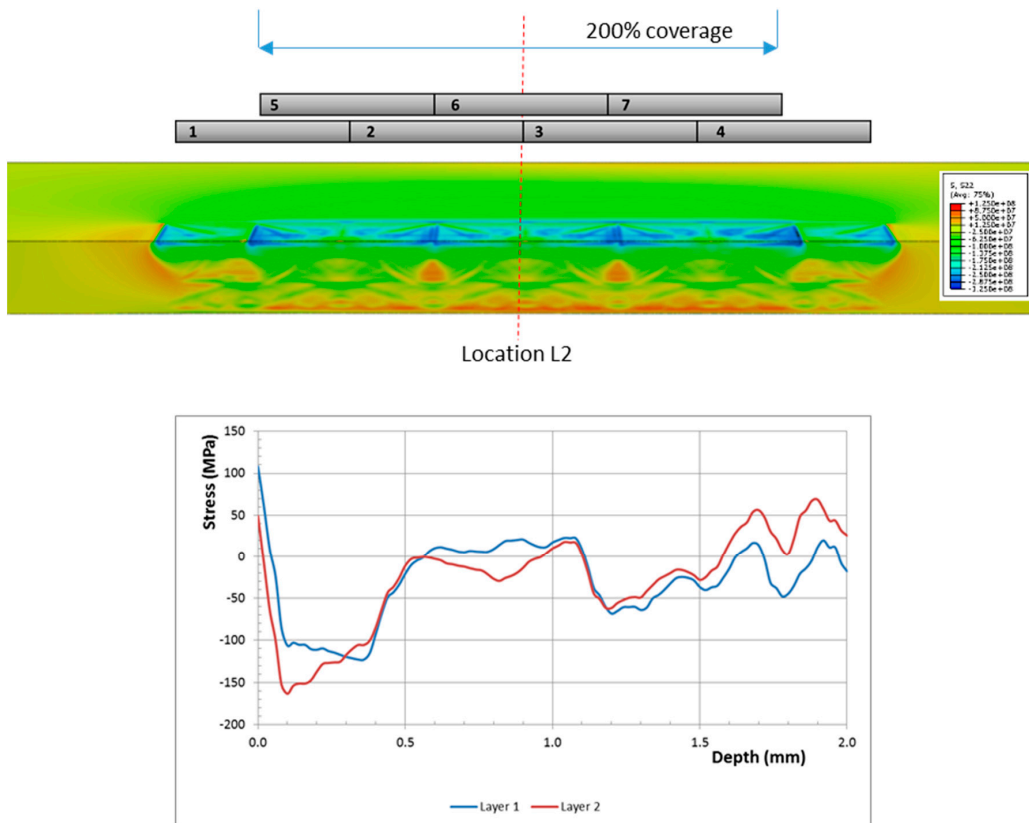


**Figure 9.** Effect of peen layering on predicted in-plane residual stress in thin sections. Stresses were extracted from the FEA model at Location L2 after one and two layers of peening.

### 3.2.3. Effects of Peen Patterning

In Figure 10, we consider the effects of altering the peen patterning while still maintaining a coverage of 300% along the central portion of the peen line. Two additional scenarios were evaluated: Pattern 2, which is similar in application to the scenario considered in Section 3.2.2 (denoted in this section as Pattern 1) but reduces the offset between layers from one-half the spot width to one-third (Figure 10a); and Pattern 3, which uses a running overlap (Figure 10b) pattern. As is shown, both of these patterns achieve exactly three layers of peening along the central portion of the peen line.

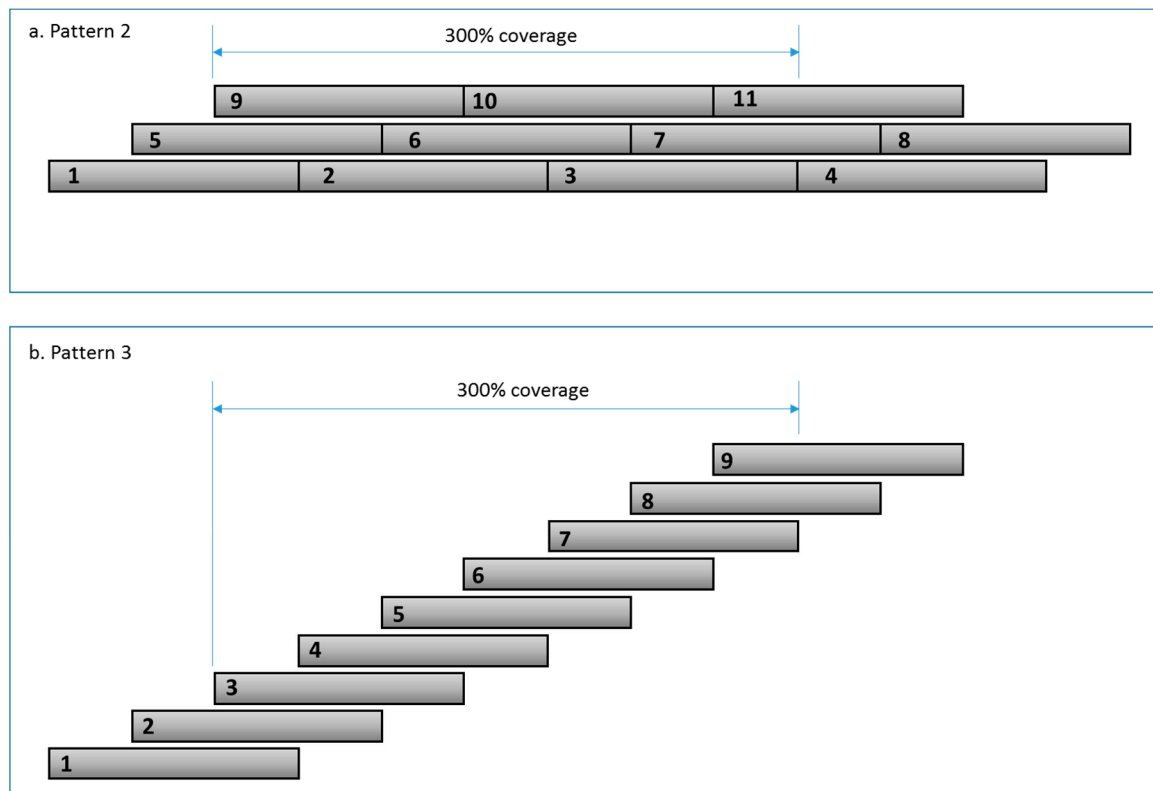


**Figure 10.** Schematics for achieving 300% peen coverage: (a) Pattern 2; (b) Pattern 3. Figure 8 shows Pattern 1.

The corresponding contour and line plots for peen Patterns 2 and 3 are shown in Figure 11. As is illustrated, decreasing the offset from one-half to one-third the spot width does not alleviate the tensile stresses at the surface. As was observed with Pattern 1, small regions of tension persist in the spot centers of the topmost layer for Pattern 2. However, the build-up of subsurface tensile stresses is significantly reduced by reducing the offset.

The running peen pattern (Pattern 3), on the other hand, does result in a complete suppression of surface and near-surface tensile stress (Figure 11b), to a depth of almost 1 mm. For the peening parameters used in the simulations, the surface stress in the spot centers decreases from about 60 MPa to about  $-135$  MPa, while the subsurface tension at mid-section decreases from a maximum of 100 MPa for Pattern 1 to about 0 MPa for Pattern 3. Note that the more compressive surface stresses observed from the running overlap pattern result from the beneficial interactions of subsequent peen spots applied over previously induced fields; for other combinations of peening parameters and specimen geometry other surface conditions may arise.

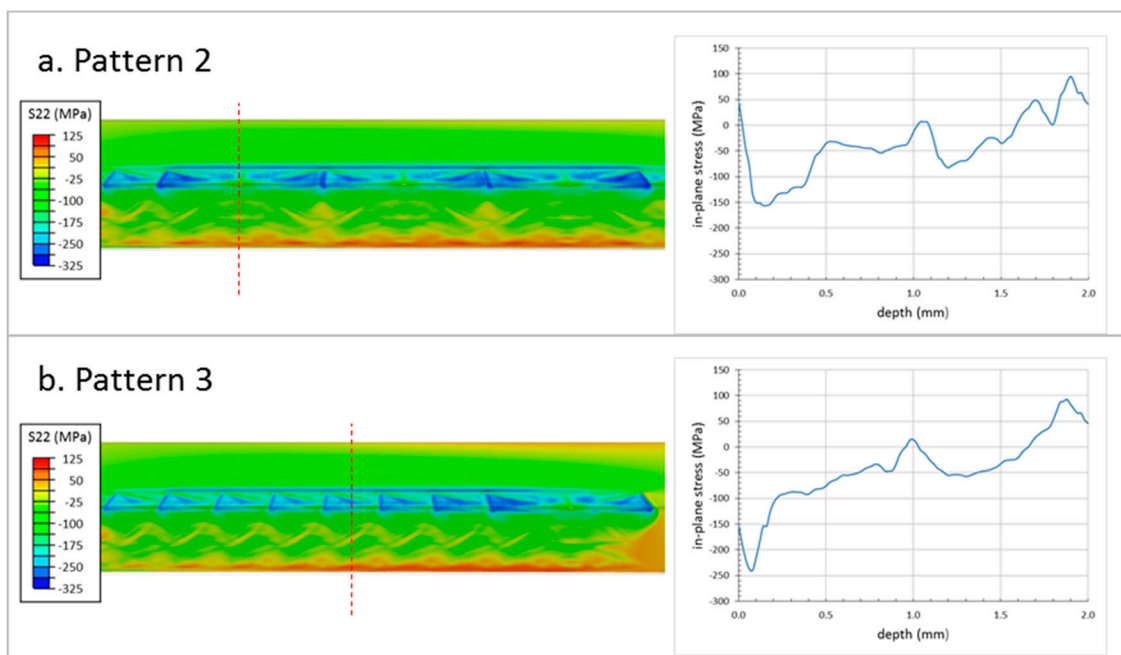


**Figure 11.** Effects of peen layering on predicted in-plane residual stress: (a) Pattern 2; (b) Pattern 3. The patterns are shown in Figure 10.

#### 4. Conclusions

In this work, finite element analysis was used to study the effects of peen patterning on the residual stress fields induced by laser peening of thin aluminum plates. The accuracy of the model was confirmed using experimental measurements of residual stress obtained by incremental hole drilling. The following conclusions can be drawn:

1. In thin plates of aluminum, above a threshold value of peak applied pressure, laser peening can lead to undesirable local “hotspots” of tensile residual stress as a consequence of the interaction of the shock wave with the geometry. In thin sections, reflected stress waves occur that, in combination with the smaller amount of constraining material, can lead to tensile stress on the peened surface through localized reverse yielding.
2. Mitigation of the tensile regions can be affected by layering of the peen spots, where additional layers can reduce the tensile zones and generate compression. However, for a given specimen or component geometry, the resultant stress fields are dependent upon the peening parameters and the precise geometry of the patterning that is applied.
3. In thin structures, the residual stresses resulting from applying multiple peen spots to a single location do not necessarily match the results obtained from applying multiple peen spots using offset peen patterning.
4. Peen patterning can affect the biaxiality of the residual stress field, most notably if a line of peen spots is generated to overlay a surface scratch, for example, where the lowest magnitude of residual stress is found to be perpendicular to the peen line.

**Author Contributions:** All authors contributed to the conceptualization, methodology, and review and editing of the manuscript. T.J.S. developed the fundamental models and parametric studies. K.L. undertook the advanced model development and simulation. M.E.F. was responsible for providing calibration and validation data, along with funding acquisition. K.L. and M.E.F. were responsible for preparation of the initial draft of the manuscript. All authors have read and agreed to the published version of the manuscript.

**Funding:** This research study was sponsored by the Air Force Office of Scientific Research, Air Force Material Command, USAF, under grant number FA8655-12-1-2084, and the Air Force Research Laboratory’s Aerospace Systems Directorate. The U.S. Government is authorized to reproduce and distribute reprints for Government

purpose notwithstanding any copyright notation thereon. The views and conclusions contained herein are those of the authors and should not be interpreted as necessarily representing the official policies or endorsements, either expressed or implied, of the Air Force Office of Scientific Research or the U.S. Government. MEF is grateful for funding from the Lloyd's Register Foundation, a charitable foundation helping to protect life and property by supporting engineering-related education, public engagement and the application of research.

**Conflicts of Interest:** The authors declare no conflict of interest.

## References

1. Tenaglia, R.D.; Lahrman, D.F. Preventing Fatigue Failures with Laser Peening. In *AMPTIAC Quarterly*; Defense Technical Information Center: Fort Belvoir, VA, USA, 2003; pp. 3–7.
2. Bair, R. Application of Surface Residual Stresses for Durability and Damage Tolerance Improvement in F-22 Wing Attachment Lugs. In Proceedings of the Aircraft Structural Integrity Program (ASIP) Conference, Jacksonville, FL, USA, 1–3 December 2009.
3. Fairand, B.P.; Wilcox, B.A.; Gallagher, W.J.; Williams, D.N. Laser shock-induced microstructural and mechanical property changes in 7075 aluminum. *J. Appl. Phys.* **1972**, *43*, 3893–3895. [[CrossRef](#)]
4. Fairand, B.P.; Clauer, A.H.; Jung, R.G.; Wilcox, B.A. Quantitative assessment of laser-induced stress waves generated at confined surfaces. *Appl. Phys. Lett.* **1974**, *25*, 431–433. [[CrossRef](#)]
5. Montross, C.S.; Wei, T.; Ye, L.; Clark, G.; Mai, Y.W. Laser shock processing and its effects on microstructure and properties of metal alloys: A review. *Int. J. Fatigue* **2002**, *24*, 1021–1036. [[CrossRef](#)]
6. Ding, K.; Ye, L. *Laser Shock Processing, Process Performance and Simulation*; CRC Press: Boca Raton, FL, USA, 2006.
7. Wu, J.; Zhao, J.; Qiao, H.; Liu, X.; Zhang, Y.; Hu, T. Acoustic wave detection of laser shock peening. *Opto Electron. Adv.* **2018**, *1*, 180016. [[CrossRef](#)]
8. US Air Force Scientific Advisory Board. *Sustaining Air Force Aging Aircraft into the 21st Century*, Report SAB-TR-11-01. 01 August 2011.
9. Clauer, A.H.; Lahrman, D.F. *Laser Shock Processing as a Surface Enhancement Process*; Durable Surfaces: Malvern, PA, USA, 2001; pp. 121–142.
10. Dorman, M.; Toparli, M.B.; Smyth, N.; Cini, A.; Fitzpatrick, M.E.; Irving, P.E. Effect of laser shock peening on residual stress and fatigue life of clad 2024 aluminium sheet containing scribe defects. *Mater. Sci. Eng. A* **2012**, *548*, 142–151. [[CrossRef](#)]
11. Bhamare, S.; Ramakrishnan, G.; Mannava, S.R.; Langer, K.; Vasudevan, V.K.; Qian, D. Simulation-based optimization of laser shock peening process for improved bending fatigue life of Ti-6Al-2Sn-4Zr-2Mo alloy. *Surf. Coat. Technol.* **2013**, *232*, 464–474. [[CrossRef](#)]
12. Smyth, N.A.; Toparli, M.B.; Fitzpatrick, M.E.; Irving, P.E. Recovery of fatigue life using laser peening on 2024-T351 aluminium sheet containing scratch damage: The role of residual stress. *Fatigue Fract. Eng. Mater. Struct.* **2019**, *42*, 1161–1174. [[CrossRef](#)]
13. Toparli, M.B.; Fitzpatrick, M.E. Residual Stresses Induced by Laser Peening of Thin Aluminium Plates. In *Materials Science Forum*; Trans Tech Publications: Zurich, Switzerland, 2011; pp. 504–509.
14. Achintha, M.N.; Nowell, D.; Shapiro, K.; Withers, P.J. Eigenstrain modelling of residual stress generated by arrays of laser shock peening shots and determination of the complete stress field using limited strain measurements. *Surf. Coat. Technol.* **2013**, *216*, 68–77. [[CrossRef](#)]
15. Cellard, C.; Reira, D.; François, M.; Rouhaud, E.; Le Saunier, D. Laser shock peening of Ti-17 titanium alloy: Influence of process parameters. *Mater. Sci. Eng. A* **2012**, *532*, 362–372. [[CrossRef](#)]
16. Toparli, M.B.; Fitzpatrick, M.E. Through Thickness Residual Stress Measurements by Neutron Diffraction and Hole Drilling in a Single Laser-Peened Spot on a Thin Aluminium Plate. In *Materials Science Forum*; Trans Tech Publications: Zurich, Switzerland, 2014; pp. 167–172.
17. Ding, K.; Ye, L. FEM simulation of two sided laser shock peening of thin sections of Ti-6Al-4V alloy. *Surf. Eng.* **2003**, *19*, 127–133. [[CrossRef](#)]
18. Hong, Z.; Chengye, Y. Laser shock processing of 2024-T62 aluminum alloy. *Mater. Sci. Eng. A* **1998**, *257*, 322–327. [[CrossRef](#)]
19. Yang, J.M.; Her, Y.C.; Han, N.; Clauer, A. Laser shock peening on fatigue behavior of 2024-T3 Al alloy with fastener holes and stopholes. *Mater. Sci. Eng. A* **2001**, *298*, 296–299. [[CrossRef](#)]

20. Ivetic, G.; Meneghin, I.; Troiani, E.; Molinari, G.; Ocana, J.; Morales, M. Fatigue in laser shock peened open-hole thin aluminium specimens. *Mater. Sci. Eng. A* **2012**, *534*, 573–579. [[CrossRef](#)]
21. Braisted, W.; Brockman, R. Finite element simulation of laser shock peening. *Int. J. Fatigue* **1999**, *21*, 719–724. [[CrossRef](#)]
22. Ding, K.; Ye, L. Three-dimensional dynamic finite element analysis of multiple laser shock peening processes. *Surf. Eng.* **2003**, *19*, 351–358. [[CrossRef](#)]
23. Ocaña, J.L.; Morales, M.; Molpeceres, C.; Torres, J. Numerical simulation of surface deformation and residual stresses fields in laser shock processing experiments. *Appl. Surf. Sci.* **2004**, *238*, 242–248. [[CrossRef](#)]
24. Singh, G.; Grandhi, R.; Stargel, D.; Langer, K. Modeling and optimization of a laser shock peening process. In Proceedings of the 12th AIAA/ISSMO Multidisciplinary Analysis and Optimization Conference, Victoria, BC, Canada, 10–12 September 2008; pp. 5838–5850.
25. Brockman, R.A.; Braisted, W.R.; Olson, S.E.; Tenaglia, R.D.; Clauer, A.H.; Langer, K.; Shepard, M.J. Prediction and characterization of residual stresses from laser shock peening. *Int. J. Fatigue* **2012**, *36*, 96–108. [[CrossRef](#)]
26. Hasser, P.J.; Malik, A.S.; Langer, K.; Spradlin, T.J. Simulation of Surface Roughness Effects on Residual Stress in Laser Shock Peening. In Proceedings of the ASME 2013 International Manufacturing Science and Engineering Conference Collocated with the 41st North American Manufacturing Research Conference: American Society of Mechanical Engineers, Madison, WI, USA, 10–14 June 2013.
27. *ABAQUS Version 6.14 User's Manual*; Dassault Systèmes: Providence, RI, USA, 2015.
28. Peyre, P.; Fabbro, R. Laser Shock Processing: A Review of the Physics and Applications. *Opt. Quantum Electron.* **1995**, *27*, 1213–1229.
29. Peyre, P.; Fabbro, R.; Merrien, P.; Lieurade, H.P. Laser shock processing of aluminium alloys. *Application to high cycle fatigue behaviour. Mater. Sci. Eng. A* **1996**, *210*, 102–113.
30. Spradlin, T.J.; Grandhi, R.V.; Langer, K. Experimental validation of simulated fatigue life estimates in laser-peened aluminum. *Int. J. Struct. Integr.* **2011**, *2*, 74–86. [[CrossRef](#)]
31. Zhou, Z.; Gill, A.S.; Qian, D.; Mannava, S.R.; Langer, K.; Wen, Y.; Vasudevan, V.K. A finite element study of thermal relaxation of residual stress in laser shock peened IN718 superalloy. *Int. J. Impact Eng.* **2011**, *38*, 590–596. [[CrossRef](#)]
32. Zhou, Z.; Bhamare, S.; Ramakrishnan, G.; Mannava, S.R.; Langer, K. Thermal relaxation of residual stress in laser shock peened Ti-6Al-4V alloy. *Surf. Coat. Technol.* **2012**, *206*, 4619–4627. [[CrossRef](#)]
33. Spradlin, T.; Grandhi, R.; Langer, K. Modified Symmetry Cell Approach for Simulation of Surface Enhancement Over Large Scale Structures. In Proceedings of the 2011: ICSP-11, South Bend, IN, USA, 12–15 September 2011; pp. 111–116.
34. Hatamleh, M.I.; Mahadevan, J.S.; Malik, A.S.; Qian, D. Variable Damping Profiles for Laser Shock Peening Simulation Using Modal ANalysis and the SEATD Method. In Proceedings of the ASME 12th International Manufacturing Science and Engineering Conference MSEC2017, Los Angeles, CA, USA, 4–8 June 2017.
35. Meyers, M.A. *Dynamic Behavior of Materials*; John Wiley & Sons: New York, NY, USA, 1994.
36. Johnson, G.R.; Cook, W.H. A constitutive model and data for metals subjected to large strains, high strain rate and high temperatures. In Proceedings of the 7th International Symposium on Ballistics, The Hague, The Netherlands, 19–20 April 1931; pp. 541–547.
37. Lesuer, D.R. *Experimental Investigations of Material Models for T-6Al-4V Titanium and 2024-T3 Aluminum*; Lawrence Livermore National Laboratory: Berkeley, CA, USA, 2000.
38. Langer, K.; Olson, S.; Brockman, R.; Braisted, W.; Spradlin, T.; Fitzpatrick, M.E. High strain-rate material model validation for laser peening simulation. *J. Eng.* **2015**, *13*, 150–157. [[CrossRef](#)]
39. Amarchinta, H.K.; Grandhi, R.V.; Langer, K.; Stargel, D.S. Material model validation for laser shock peening process simulation. *Model. Simul. Mater. Sci. Eng.* **2009**, *17*, 015010. [[CrossRef](#)]
40. Amarchinta, H.K.; Grandhi, R.V.; Clauer, A.H.; Langer, K.; Stargel, D.S. Simulation of residual stress induced by a laser peening process through inverse optimization of material models. *J. Mater. Process. Technol.* **2010**, *210*, 1997–2006. [[CrossRef](#)]
41. Angulo, I.; Cordovilla, F.; García-Beltrán, A.; Smyth, N.S.; Langer, K.; Fitzpatrick, M.E.; Ocaña, J.L. The effect of material cyclic deformation properties in residual stress generation by laser shock processing. *Int. J. Mech. Sci.* **2019**, *156*, 370–381. [[CrossRef](#)]
42. Fabbro, R.; Fournier, J.; Ballard, P.; Devaux, D.; Virmont, J. Physical study of laser-produced plasma in confined geometry. *J. Appl. Phys.* **1990**, *68*, 775–784. [[CrossRef](#)]

43. Ocaña, J.L.; Morales, M.; Molpeceres, C.; Torres, J.; Porro, J.A.; Gomez, G.; Rubio, C. Predictive assessment and experimental characterization of the influence of irradiation parameters on surface deformation and residual stresses in laser shock processed metallic alloys. *High Power Laser Ablation V* **2004**, *5548*, 642–653.
44. Morales, M.; Ocaña, J.L.; Molpeceres, C.; Porro, J.A.; García-Beltrán, A. Model based optimization criteria for the generation of deep compressive residual stress fields in high elastic limit metallic alloys by ns-laser shock processing. *Surf. Coat. Technol.* **2008**, *202*, 2257–2262. [[CrossRef](#)]
45. Ocaña, J.L.; Morales, M.; Molpeceres, C.; Porro, J.A. Laser Shock Processing of Metallic Materials: Coupling of Laser-Plasma Interaction and Material Behaviour Models for the Assessment of Key Process Issues. *High Power Laser Ablation* **2010**, *1278*, 902–913.
46. Morales, M.; Correa, C.; Porro, J.; Molpeceres, C.; Luis Ocaña, J. Thermomechanical modelling of stress fields in metallic targets subject to laser shock processing. *Int. J. Struct. Integr.* **2011**, *2*, 51–61. [[CrossRef](#)]



© 2020 by the authors. Licensee MDPI, Basel, Switzerland. This article is an open access article distributed under the terms and conditions of the Creative Commons Attribution (CC BY) license (<http://creativecommons.org/licenses/by/4.0/>).